

## Article

# Adsorption of Low-Concentration Ammonia Nitrogen from Water on Alkali-Modified Coal Fly Ash: Characterization and Mechanism

Yuyan Zhao <sup>1,2</sup> , Hanwen Luan <sup>1</sup>, Binghan Yang <sup>1</sup>, Zhenghe Li <sup>1</sup>, Meitong Song <sup>1</sup>, Bing Li <sup>1,2</sup> and Xiaodan Tang <sup>1,2,\*</sup> 

<sup>1</sup> College of Geo-Exploration Science and Technology, Jilin University, Changchun 130026, China

<sup>2</sup> Institute for Black Soils, Jilin University, Changchun 130026, China

\* Correspondence: tangxiaodan@jlu.edu.cn

**Abstract:** The huge annual output of coal fly ash is harmful to the environment, but it is widely used because of its good adsorption potential. In this study, using coal fly ash as a raw material and sodium hydroxide as an activator, a novel adsorbent was synthesized at 300 °C and used to adsorb low concentrations of ammonia nitrogen from water. In this study, scanning electron microscopy, X-ray diffraction analysis, Fourier transform infrared spectroscopy, energy dispersive X-ray spectroscopy, and a surface area and porosity analyzer were used to analyze the adsorbent's physicochemical properties. The results showed that after alkali modification, the activity of the adsorbent had greatly enhanced. The impacts of solution pH, adsorbent dosage, adsorption time, and initial concentration of ammonia nitrogen on the adsorption capacity and removal efficiency were evaluated through a series of adsorption experiments. Moreover, the adsorption data were better fitted to the pseudo-second-order kinetic model and Langmuir model, indicating that the adsorption process was mainly chemical adsorption and monolayer uniform adsorption. As a result, the new adsorbent is inexpensive and effective, and it could be used to remove low-concentration ammonia nitrogen from water with a maximum removal efficiency of approximately 89%.



**Citation:** Zhao, Y.; Luan, H.; Yang, B.; Li, Z.; Song, M.; Li, B.; Tang, X. Adsorption of Low-Concentration Ammonia Nitrogen from Water on Alkali-Modified Coal Fly Ash: Characterization and Mechanism. *Water* **2023**, *15*, 956. <https://doi.org/10.3390/w15050956>

Academic Editors: Stanislav Frančišković-Bilinski and Sanja Sakan

Received: 1 December 2022

Revised: 19 February 2023

Accepted: 27 February 2023

Published: 1 March 2023



**Copyright:** © 2023 by the authors. Licensee MDPI, Basel, Switzerland. This article is an open access article distributed under the terms and conditions of the Creative Commons Attribution (CC BY) license (<https://creativecommons.org/licenses/by/4.0/>).

## 1. Introduction

Ammonia nitrogen exists in two forms in water, one is ionized ammonia ( $\text{NH}_4^+$ ) and the other is non-ionized ammonia ( $\text{NH}_3$ ) [1]. Water eutrophication may result from a high level of ammonia nitrogen, and the oxidation of ammonia nitrogen lowers the amount of dissolved oxygen in water, causing the water body to become black and smelly, and the water quality to deteriorate [2]. The remediation of ammonia nitrogen pollution in water has always been a promising research area in environmental engineering. Ammonia nitrogen concentration in water can be decreased in a variety of ways, including air stripping [3], biological nitrification–denitrification [4], chemical precipitation [5], breakpoint chlorination [6], membrane technology [7], electrochemical oxidation [8], ion exchange, and adsorption methods [9]. Among them, the adsorption approach is the most popular, since the reaction process is uncomplicated, steady, and manageable, and the selected adsorbent can be cheap, renewable, and reusable [10].

Common adsorbents for the remediation of wastewater contaminated by ammonia nitrogen include clay minerals, zeolite minerals, and biological adsorbents. As a cation exchanger [11], zeolite has an abundant pore structure and strong adsorption capacity, and it is widely used to remove heavy metal ions and ammonia nitrogen [12,13]. As a kind of industrial solid waste, Coal fly ash (CFA) can form various crystal forms of zeolite after modification, which has attracted more and more attention. As much as 750 million

tons of CFA are created annually worldwide from the burning of coal [14,15]. CFA has been widely used as an alternative to traditional adsorbents due to its large quantity, low cost, easy biodegradability, and characteristic structural (including porosity, bulk density, and surface) properties [16,17]. However, the dense glassy structure produces a protective layer on the exterior of CFA, which inhibits the potential chemical activity and adsorption capacity of CFA; therefore, it is necessary to modify and activate CFA in order to boost its adsorption capacity [18]. CFA can be synthesized into various crystalline zeolites through different modification techniques [19], and the modified CFA can be used to treat volatile organic matter, heavy metal ions, ammonia nitrogen, and phosphorus [20,21]. Hydrothermal synthesis, melting, supercritical treatment and some other processes are the ways to achieve CFA activation. When the CFA is modified and activated as a strong adsorbent to treat ammonia nitrogen in wastewater, it allows for the treatment of waste with waste and the utilization of waste resources.

The reduction of ammonia nitrogen pollution in bodies of water has long been a focus of scientific inquiry. Various modifications have been made to naturally porous minerals, such as zeolite and montmorillonite [22–24], to increase their effectiveness in adsorbing ammonia nitrogen. The novel zeolitization ceramsite from industrial wastes was synthesized by a green process of high temperature sintering activation and hydrothermal reaction; its specific surface area was increased from  $1.259\text{ m}^2/\text{g}$  to  $17.92\text{ m}^2/\text{g}$ , and its maximum adsorption capacity of ammonia nitrogen reached  $19.9\text{ mg/g}$  [25]. Synthetic manganese oxides prepared from the redox reaction between  $\text{KMnO}_4$  and  $\text{MnSO}_4$  were used to remove ammonia nitrogen from aqueous solutions, and it was found that the highest adsorption capacity would occur at  $\text{pH} = 6$ , and the removal efficiency reached 87.9% [26]. Durian biomass fiber modified with Cu-Al bimetallic oxide (Cu-Al/DBF) was synthesized by a hydrothermal reaction, and its maximum adsorption capacity for ammonia nitrogen was  $18.04\text{ mg/g}$  [27]. Cheng's group [14,28] studied the adsorption efficiency of CFA modified with different structures on the experimentally simulated ammonia nitrogen wastewater with different concentrations. Bentonite was modified by aluminum cross-linking and tannin double modification; its adsorption capacity for the simulated high-concentration ammonia nitrogen was  $5.85\text{ mg/g}$ , and its ammonia nitrogen adsorption process was found to be similar to that of modified CFA [29]. The adsorbent for ammonia nitrogen is numerous; however, the current focus of research into this material's adsorption is on high-concentration ammonia nitrogen pollution, with little attention paid to the issue of relatively low-concentration (about  $10\text{ mg/L}$ ) ammonia nitrogen pollution.

In this article, CFA was used as a raw material and sodium hydroxide ( $\text{NaOH}$ ) was used as an activator. Through low temperature roasting modification, a new type of modified adsorbent was obtained to address the issue of low-concentration ammonia nitrogen pollution in water. The techniques of scanning electron microscope (SEM), energy dispersive X-ray spectroscopy (EDS), surface area and porosity analyzer (BET), X-ray diffraction analysis (XRD), and Fourier transform infrared spectroscopy (FT-IR) were introduced to characterize the chemical and physical performance of the samples. A series of ammonia nitrogen adsorption simulation experiments were carried out and the impacts of different initial concentrations, adsorbent dosages, adsorption time and solution pH on equilibrium adsorption capacity and adsorption efficiency were analyzed, and the adsorption mechanism was also studied.

## 2. Materials and Method

The schematic diagram of the  $\text{NaOH}$ -CFA preparation, performance characterization, and adsorption analysis is shown in Figure 1.

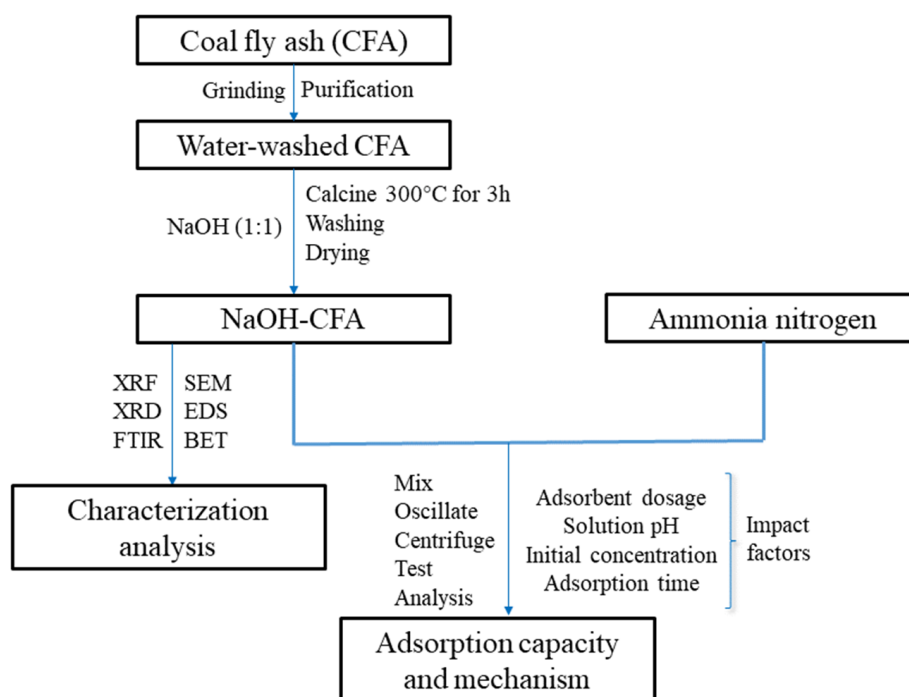


**Figure 1.** Scheme of NaOH-CFA preparation, performance characterization, and adsorption analysis.

## 2.1. Experiment Materials and Instruments

The CFA used in this experiment came from a coal-fired power station in Jilin City. Its main components were SiO<sub>2</sub> (52.00 wt%), Al<sub>2</sub>O<sub>3</sub> (24.60 wt%), Fe<sub>2</sub>O<sub>3</sub> (3.74 wt%), CaO (3.08 wt%), MgO (0.53 wt%), and Na<sub>2</sub>O (0.41 wt%).

NaOH, ammonium chloride, (NH<sub>4</sub>Cl) and other reagents were of analytical grade. Hydrochloric acid (HCl) and absolute ethanol were both of confirmed analytical grade. The water used in the experiment was ultrapure deionized water. The national standard ammonia nitrogen solution (GSB04-2832-2011) was 1000 mg/L, and its solvent was ultrapure deionized water.

Using a planetary ball mill (QM-3SP4, Laibu, Nanjing, China), samples were ground into powder before being quantified by an electronic balance (ATY124, Shimadzu, Kyoto, Japan). The sample processing stage involved the use of the following equipment: the multi-head magnetic stirrer (HJ-6, Jiangnan, Jintan, China), cyclotron oscillator (HY-8A, Jingda, Jintan, China), muffle furnace (KBF1400, Laibu, Nanjing, China), pH meter (PHBJ-260, Leici, Shanghai, China), and centrifuge (TDL-5A, Anting, Shanghai, China). A fully automatic flow injection analyzer (FIA-6000+, Jitian, Beijing, China) was used to measure the ammonia nitrogen concentration. The surface structure, chemical element, main mineral composition, chemical bonding, and specific surface area of the sample were characterized by field emission SEM (JSM-7900F, JEOL, Kyoto, Japan), EDS (EDX6000B, Skyray, Kunshan, China), polycrystalline XRD (XD6, Persee, Beijing, China), FT-IR (Nicolet iS10, Thermo Scientific, Waltham, MA, USA), and BET (ASAP2020HD88, Mike, Norcross, GA, USA), respectively.

## 2.2. Preparation of Modified CFA

A 10% (*w/v*) mixture of CFA and ultrapure deionized water were combined uniformly in a beaker at 25 °C, and the combined solution was uniformly stirred in a magnetic stirrer at 120 rpm for 24 h. The precipitate was obtained by centrifuging the resulting mixture at 9000 rpm for 30 min, washed 3 times with absolute ethanol, and thoroughly cleaned numerous times with ultrapure deionized water. The obtained CFA was dried at 65 °C for 6 h, filtered through a 0.25 mm standard sieve, and preserved in the desiccator. The resulting CFA was referred to as water-washed CFA for short.

Water-washed CFA and NaOH were coupled in a weight ratio of 1:1; the mixture was calcined in the muffle furnace at 300 °C for 3 h. The roasted sample was cooled, repeatedly washed with ultrapure deionized water, and mixed for 48 h with a specific amount of ultrapure deionized water, and then the sample was separated from the liquid. Finally, a 0.25 mm sieve was used to screen the dried sodium hydroxide-modified CFA (NaOH-CFA). The comparison images of CFA, water-washed CFA, and NaOH-CFA are shown in Figure 2. The three materials were all gray powders. The NaOH-CFA was lighter in color than the water-washed CFA and NaOH-CFA, and its particle size was finer than the other two materials.

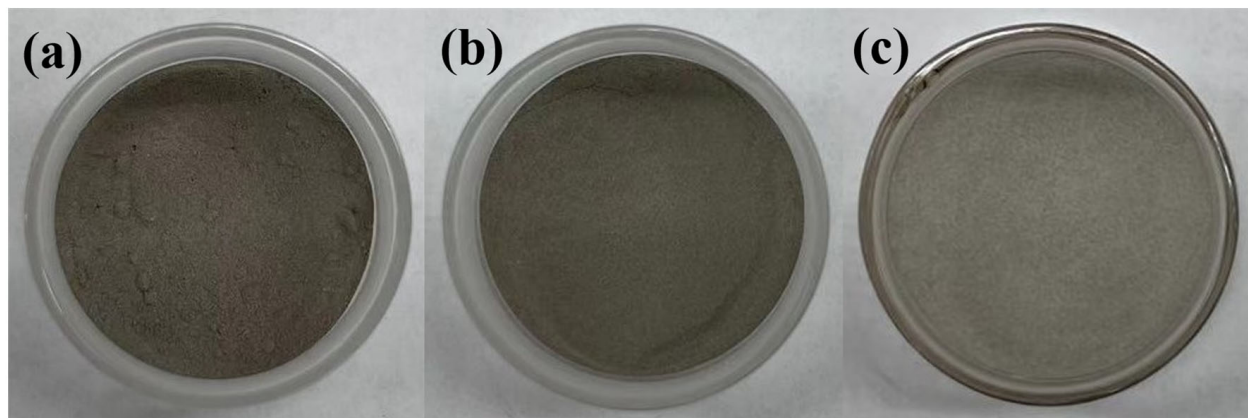


**Figure 2.** Material images of (a) CFA; (b) water-washed CFA; and (c) NaOH-CFA.

### 2.3. Batch Sorption Experiments

A convex flask was filled with 100 mL ammonia nitrogen solution at a specific concentration. Its initial pH was then changed using 0.1 mol/L HCl or 0.1 mol/L NaOH according to the experimental requirements. Then, a specific quantity of NaOH-CFA was poured into the convex flask, shaken for a specified period of time at 180 rpm while at room temperature, and percolated through a 0.45 µm membrane; finally, the obtained solution was diluted into the colorimetric tube for the flow injection analyzer test.

In order to study the impact of pH, it was changed to 2, 3, 4, 5, 6, 7, 8, 9, 10, 11, and 12, with 1.0 g of NaOH-CFA dosage, 90 min of adsorption time and 10 mg/L ammonia nitrogen solution.

To analyze the effect of adsorbent dosage, NaOH-CFA was weighed at 0.1 g, 0.2 g, 0.4 g, 0.8 g, 1.0 g, and 1.5 g with pH 7, 90 min of adsorption time and 10 mg/L ammonia nitrogen solution.

With pH of 7, 1.0 g of NaOH-CFA dosage, and 10 mg/L ammonia nitrogen solution, the adsorption kinetics experiment was conducted at the adsorption times of 5 min, 10 min, 20 min, 30 min, 45 min, 60 min, 90 min, 120 min, and 180 min.

A pH of 7, 1.0 g of NaOH-CFA dosage, and 90 min of adsorption time were used to study the effect of initial ammonia nitrogen concentrations of 5 mg/L, 10 mg/L, 20 mg/L, 30 mg/L, 50 mg/L, and 100 mg/L.

The adsorption capacity  $Q$  (mg/g) and removal efficiency  $R$  (%) of ammonia nitrogen were calculated by Equations (1) and (2) [30], respectively.

$$Q = \frac{C_0 - C_t}{m} \times \frac{V}{1000} \quad (1)$$

$$R = \frac{C_0 - C_t}{C_0} \times 100\% \quad (2)$$

where  $C_0$  (mg/L) is the initial ammonia nitrogen concentration,  $C_t$  (mg/L) is the ammonia nitrogen concentration at time  $t$  (min),  $V$  (mL) is the solution volume, and  $m$  (g) is the mass of NaOH-CFA.

In brief, the batch sorption experiments were conducted by changing the NaOH-CFA dosage, initial ammonia nitrogen concentration, solution pH, and adsorption time of the system. The experimental data were analyzed and plotted using analyses of variance and regression in Excel and Origin. The coefficient of variation was mostly less than 1%. If the variation in element content exceeded 5%, an identical run would be undertaken and closer data points would be used. All mean values were the averages of three independent samples. Blank and parallel controls were set in the experiment.

### 3. Results and Discussion

#### 3.1. Material Characterization

##### 3.1.1. SEM Analysis

As shown in Figure 3, the structure of CFA and NaOH-CFA is completely different. CFA had a smooth surface and its main morphology was amorphous aluminosilicate glass spheres [30], which varied in size from a few microns to 30 microns. The original lattice of CFA got broken after NaOH and CFA were well-mixed and reacted at 300 °C, and its microstructure changed from a spherical block structure to a porous material structure. The pores of the NaOH-CFA (Figure 3b) were well developed, which promoted the increase of specific surface area and the number of ion exchange sites; hence, the adsorption capacity of the NaOH-CFA improved. In Figure 3c, after the NaOH-CFA adsorbed ammonia nitrogen, there were still residual pores on its surface, suggesting its excellent adsorption effect. The ions were exchanged through pores, so the surface morphology did not undergo any obvious changes.

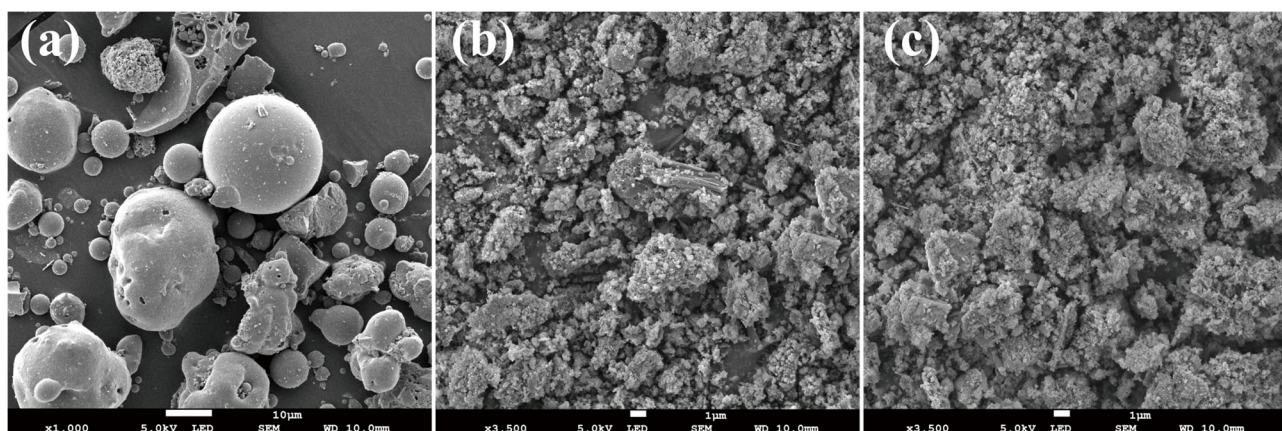


**Figure 3.** Morphology images of (a) CFA; (b) NaOH-CFA; and (c) NaOH-CFA adsorbing ammonia nitrogen.

##### 3.1.2. EDS Analysis

The chemical elements of CFA and NaOH-CFA before and after ammonia nitrogen adsorption were measured by EDS, as shown in Figure 4. The main chemical elements of CFA in Figure 4a were C, O, Si, and Al. In Figure 4b, it can be seen that the major chemical elements of the NaOH-CFA were the same as CFA, but the peak heights of Al and Si decreased visibly, and the C content was relatively lower. The rise of the Na peak indicated that the Na from NaOH was exchanged onto the surface of the NaOH-CFA through modification. After the NaOH-CFA adsorbed ammonia nitrogen, the peak of N could be seen in Figure 4c, revealing that ammonia nitrogen was attached to the adsorbent surface.

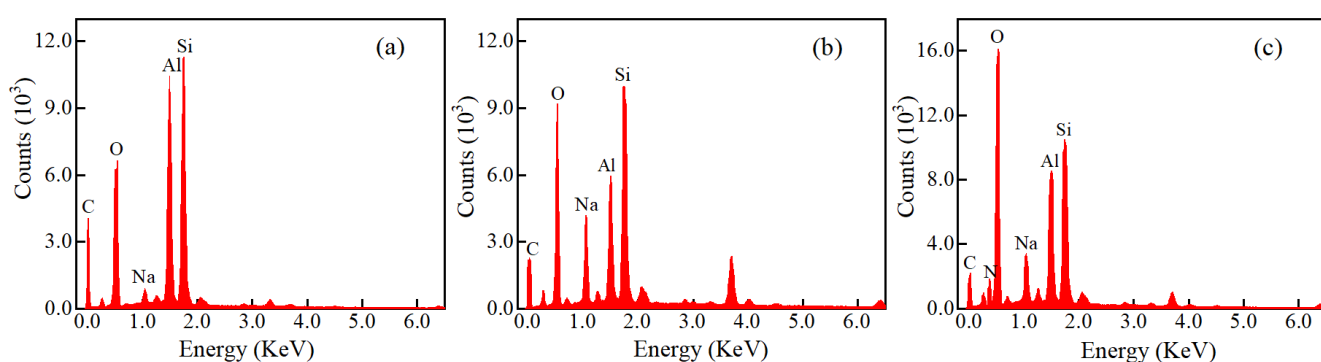


**Figure 4.** Energy spectra of (a) CFA; (b) NaOH-CFA; and (c) NaOH-CFA adsorbing ammonia nitrogen.

### 3.1.3. BET Analysis

The primary factor impacting the adsorption capacity was the specific surface of the adsorbent. The hysteresis curves of the CFA and NaOH-CFA in Figure 5 were obtained using BET. As the relative pressure rose, the hysteresis curve of CFA remained flat, and the adsorption per unit mass had almost no change, indicating that CFA itself had fewer pores and a smaller specific surface area [31]. Conversely, the unit mass adsorption of the NaOH-CFA gradually increased with the increase of relative pressure. As the relative pressure ( $P/P_0$ ) was lower than 0.4, the curve of the NaOH-CFA was also flat, but when it exceeded 0.4, the curve increased sharply. The  $N_2$  desorption occurred more easily in the NaOH-CFA compared to the CFA, which meant that the NaOH-CFA had relatively larger mesopores. The specific surface area of CFA was  $0.68 \text{ m}^2/\text{g}$ , and after being modified at  $300^\circ\text{C}$  with NaOH, it increased to  $20.22 \text{ m}^2/\text{g}$ , which was 30 times more. After NaOH reacted with  $\text{SiO}_2$ ,  $\text{Al}_2\text{O}_3$ , and other oxides, a dense cavity structure could emerge, increasing the specific surface area of the NaOH-CFA. As the CFA particles were opened, more active sites were released, and the crystalline phase in CFA was transformed into an amorphous state.

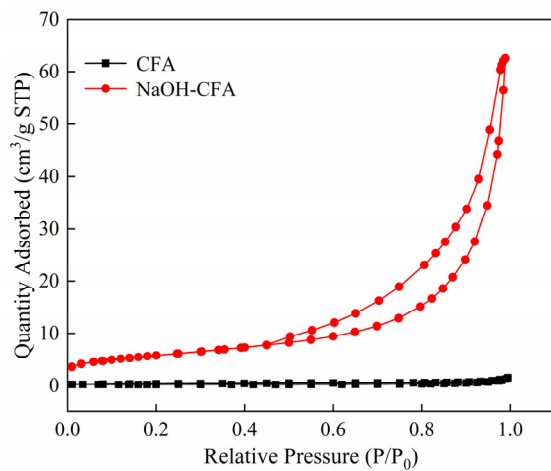


**Figure 5.** Relative quantity adsorbed of the CFA and NaOH-CFA.

### 3.1.4. XRD Analysis

As shown in Figure 6, the main mineral components of CFA were quartz and mullite ( $\text{Al}_6\text{Si}_2\text{O}_{13}$ ) [32]. After modification, the contents of quartz and mullite were significantly reduced, and no new minerals were produced. As the main oxides of CFA reacted with NaOH, the internal structure of CFA was destroyed and a new porous structure was formed, which was similar to the structure of the crystallized zeolite. This phenomenon revealed that the spherical block structure of CFA was progressively cracked as a result of the reaction of  $\text{Al}_2\text{O}_3$ ,  $\text{SiO}_2$ , and other oxides with NaOH in the melting state, resulting in

the dissolution of active groups from CFA and the retention of only amorphous structures; this conclusion was consistent with that of SEM.

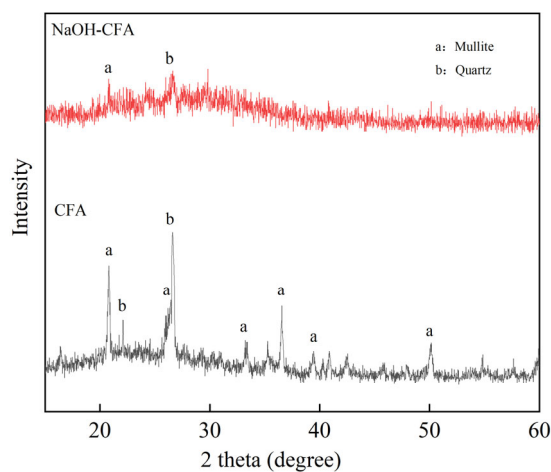


**Figure 6.** XRD diffractograms of CFA and NaOH-CFA.

### 3.1.5. FT-IR Analysis

As shown in Figure 7, CFA showed several obvious changes after modification. At  $3450\text{ cm}^{-1}$ , the peak intensity was related to  $-\text{OH}$  stretching vibration, and intermolecular hydrogen bonds were increased significantly due to the addition of NaOH. At  $1650\text{ cm}^{-1}$ , it represented the bending vibration of H-OH, and it decreased after modification, which could increase CFA adsorption capacity. The sharp peak of CFA at around  $1080\text{ cm}^{-1}$  was caused by the stretching vibration of  $\text{SiO}_4$  or  $\text{AlO}_4$  [33], and that of the NaOH-CFA decreased obviously since the internal structure was changed during the modification. At  $820\text{ cm}^{-1}$ , the stretching vibration from O-Si-O appeared. The peaks at around  $460\text{ cm}^{-1}$  denoted the bending vibration of the Si-O-Si [34].

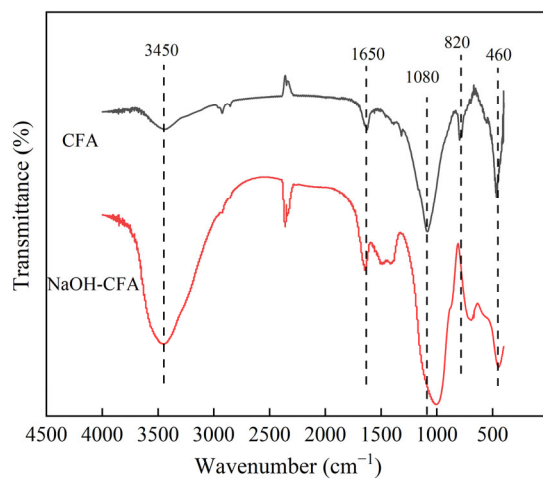


**Figure 7.** FT-IR spectra of CFA and NaOH-CFA.

To summarize, the physicochemical characteristics of CFA and NaOH-CFA were tested by various characterization instruments. CFA had a smooth spherical block structure,  $\text{SiO}_2$  and  $\text{Al}_2\text{O}_3$  accounted for a large proportion in the oxide composition, and the main minerals were quartz and mullite. After modification with NaOH, the surface morphology of CFA became irregular aggregates of porous structures, and the surface area of the NaOH-CFA was approximately 30 times greater than that of CFA; furthermore, the main chemical elements of Al and Si were reduced, the Na element was increased, and the main mineral components of quartz and mullite were also reduced, but no new mineral phases appeared.

The stretching vibrations from hydroxyl groups of Si-OH and Al-OH were enhanced. These indicated that as NaOH reacted with  $\text{SiO}_2$ ,  $\text{Al}_2\text{O}_3$  and other oxides, Si-O and Al-O bonds of CFA were destroyed, and sodium ions were exchanged onto the surface of the NaOH-CFA, which increased its adsorption capacity.

### 3.2. Adsorption Mechanism of NaOH-CFA on Low-Concentration Ammonia Nitrogen

#### 3.2.1. Impact of pH

During the adsorption experiment of ammonia nitrogen solution (10 mg/L) in Figure 8, as the pH value adjusted from 2 to 5, the ammonia nitrogen removal efficiency and the equilibrium adsorption capacity were enhanced, and they both reached maximum values when the pH was between 6 and 8 [34,35]. As the pH was increased from 8 to 12, the ability to adsorb ammonia nitrogen began to decrease dramatically. This result could be explained as follows: when the pH was 2~5, the concentration of  $\text{H}^+$  was high, and  $\text{NH}_4^+$  competed with  $\text{H}^+$  for adsorption sites; when the pH was 6~8,  $\text{NH}_4^+$  was largely exchanged as ions on the surface of the adsorbent; when the pH was 9~12, the dissociation reaction of  $\text{NH}_4^+$  in the aqueous solution was promoted, and the content of  $\text{NH}_4^+$  in the solution was continuously reduced, which weakened the ion exchange capacity of the NaOH-CFA. At the same time, it could also be explained by the zero electric point [36]. Ammonia nitrogen was in the cationic valence state in the solution when the pH was below the isoelectric point. Moreover, the NaOH-CFA surface had lots of positive charges, and the existence of charge repulsion inhibited the adsorption behavior. As the pH was higher than the isoelectric point, many negative charges were gathered at the surface of the NaOH-CFA, and the driving force of charge attraction improved the adsorption behavior, but the too high pH would promote the dissociation reaction of  $\text{NH}_4^+$  in the aqueous solution; hence, pH = 7 was selected for the subsequent experiments.

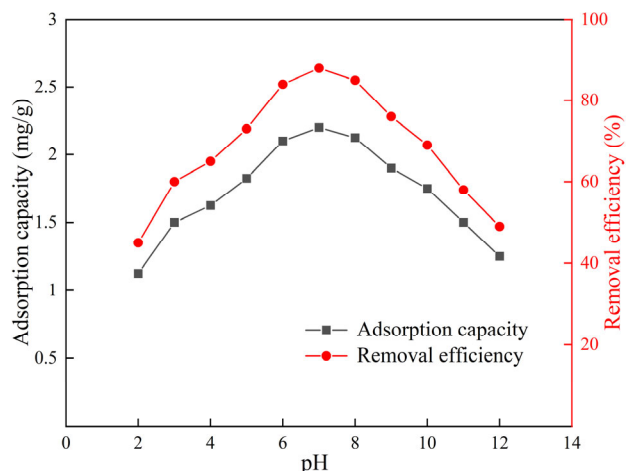


**Figure 8.** Impact of pH on adsorption of ammonia nitrogen by NaOH-CFA.

#### 3.2.2. Influence of NaOH-CFA Dosage

As shown in Figure 9, as the NaOH-CFA dosage increased, the adsorption capacity gradually decreased, but the removal efficiency gradually increased, and maintained equilibrium after the NaOH-CFA dosage reached 1.0 g. As the NaOH-CFA dosage improved, the equilibrium adsorption capacity reduced, which was related to the superposition or aggregation of adsorption sites and the further reduction of the adsorbable area. When the NaOH-CFA dosage was low, the distance between particles was large; hence, there was more  $\text{NH}_4^+$  aggregation around each particle to facilitate the effective ion exchange between the NaOH-CFA and  $\text{NH}_4^+$ ; as a result, the increase of the NaOH-CFA dosage provided more adsorption sites and could therefore increase the removal efficiency and the number of ion exchange sites [37]. However, when the NaOH-CFA dosage reached a certain level, its distribution density in solution attained a certain value, the distance

between particles became smaller, the available adsorption sites decreased, and the effective ion exchanges between the NaOH-CFA and  $\text{NH}_4^+$  were lowered, which led to a decrease in ion exchange capacity. The high concentration of adsorbent created a shielding effect on the periphery, preventing the combination of the adsorbate and adsorption site, and thus reducing the adsorption capacity. Therefore, the NaOH-CFA dosage of 1.0 g was chosen for the subsequent experiments.

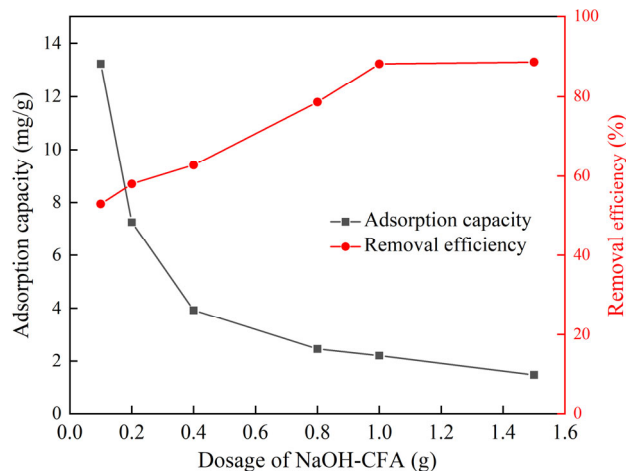


**Figure 9.** Influence of NaOH-CFA dosage on ammonia nitrogen adsorption.

### 3.2.3. Adsorption Kinetics

It can be seen in Figure 10 that the adsorption capacity of ammonia nitrogen increased rapidly with time in the first hour, and then gradually reached equilibrium. In the fast adsorption stage, the adsorption capacity was basically proportional to the time. This was primarily caused by the fact that the NaOH-CFA had a lot of ion exchange sites at the beginning of the adsorption period, which made it easy for  $\text{NH}_4^+$  to move quickly to active vacancies. As the active sites were gradually occupied, the adsorption rate decreased, and the adsorption capacity reached a stable stage. Finally, the dynamic adsorption equilibrium was maintained on the NaOH-CFA surface, and the adsorption kinetic curve became a straight line, indicating that the adsorption capacity reached the maximum value.

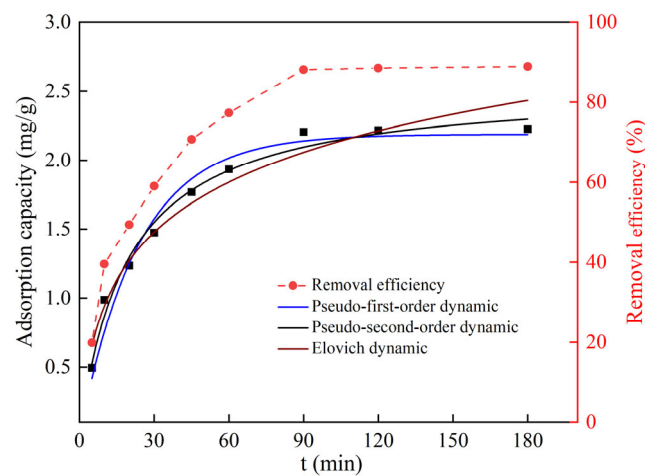


**Figure 10.** Kinetic fitting of NaOH-CFA on ammonia nitrogen adsorption.

The pseudo-first-order, pseudo-second-order and Elovich kinetic models were used to describe how the adsorption capacity changes with time. Through the kinetic analysis results, the adsorption mechanism could also be analyzed. The pseudo-second-order kinetic's optimal correlation coefficient (0.9887) was better than the pseudo-first-order

kinetic's (0.9663) and the Elovich kinetic's (0.9589). Therefore, the process of the adsorption capacity changing with time could be better simulated by the pseudo-second-order kinetic model, which indicated that chemisorption was the primary adsorption method, that the ion exchange mainly occurred on the surface of the NaOH-CFA, and that the process was an exothermic adsorption [38].

### 3.2.4. Influence of Initial Concentration

According to Figure 11, as the initial ammonia nitrogen concentration grew, the equilibrium adsorption capacity of ammonia nitrogen gradually increased. This could occur because the NaOH-CFA dosage remained unchanged. As the  $\text{NH}_4^+$  increased, more adsorption sites on the NaOH-CFA surface were occupied; but when the initial concentration was too high, the adsorption sites were fully occupied and the equilibrium adsorption capacity did not increase. However, the removal efficiency was mainly on a downward trend when the initial ammonia nitrogen concentration increased, that is, 1.0 g of NaOH-CFA was only sufficient to adsorb low concentrations of ammonia nitrogen, and as the  $\text{NH}_4^+$  increased, it would improve the dosage of NaOH-CFA to increase the removal efficiency.

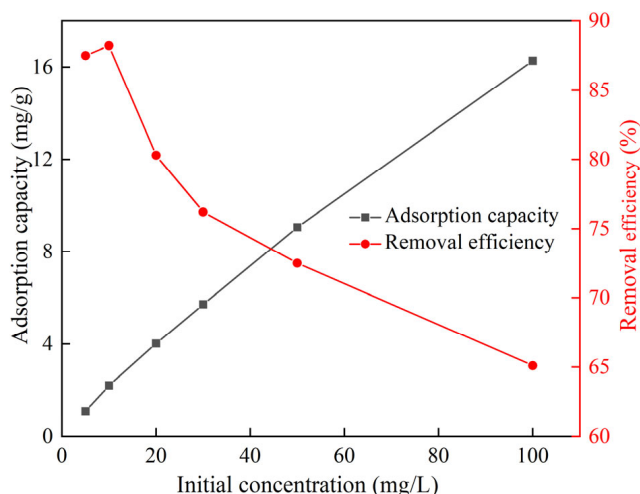


**Figure 11.** Influence of initial ammonia nitrogen concentration on adsorption.

The data of adsorption capacity changing with initial concentration were fitted by the Freundlich, Langmuir and Sips models to find the most suitable adsorption model [39]. The applicability of the three isotherms in Figure 12 was evaluated by the correlation coefficient. When the temperature was 25 °C, the Langmuir isotherm's correlation coefficient (0.9988) was higher than the Freundlich isotherm's coefficient (0.9867) and the Sips isotherm's coefficient (0.9976), demonstrating that the Langmuir isotherm was more appropriate for characterizing the experimental results. Therefore, the NaOH-CFA had a uniform surface and was more inclined to monolayer adsorption.

According to the adsorption experiment data, at an adsorption time of 90 min, 1.0 g of NaOH-CFA was sufficient to remove 10 mg/L ammonia nitrogen in the neutral system. The dosage of NaOH-CFA should be varied with the different initial ammonia nitrogen concentrations to reach the dynamic adsorption equilibrium. Through the analysis of adsorption kinetic and isotherm, the adsorption process of ammonia nitrogen by NaOH-CFA was found to be more in line with the pseudo-second-order kinetic and Langmuir isotherm. In other words, the adsorbent surface was uniform, and the chemical adsorption was the primary adsorption way.

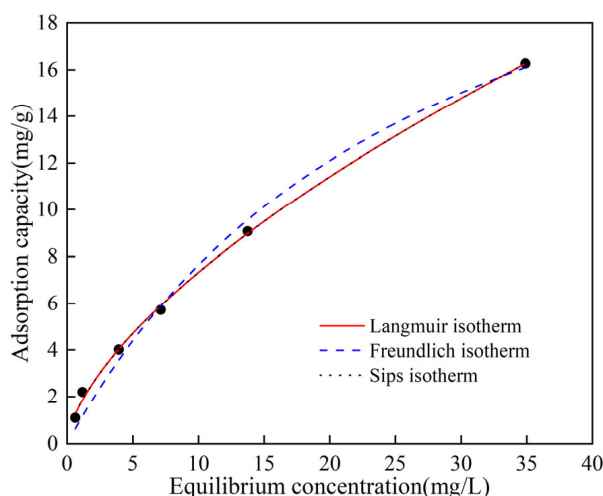


**Figure 12.** Adsorption isotherm of ammonia nitrogen on NaOH-CFA.

#### 4. Conclusions

Coal fly ash was a kind of bulk solid waste. In this study, a high efficiency ammonia nitrogen adsorbent was synthesized through a simple and economical roasting modification method. After modification, the internal glass grid structure of CFA was broken, and its specific surface area was increased from  $0.68 \text{ m}^2/\text{g}$  to  $20.22 \text{ m}^2/\text{g}$ , which was a thirtyfold increase. The activity and the adsorption sites of CFA were significantly enhanced; as a result, the adsorption capacity of ammonia nitrogen was greatly improved.

In the batch sorption experiments, the removal efficiency of ammonia nitrogen reached a maximum of 89% with a NaOH-CFA dosage of 1.0 g, ammonia nitrogen concentration of 10 mg/L, pH of 7, and adsorption time of 90 min, which could effectively address the problem of water contamination caused by a low concentration of ammonia nitrogen.

As an industrial waste, CFA is produced in large quantities every year and has a certain degree of pollution. After modification, it becomes an efficient adsorbent, turns waste into treasure, and it has wide-ranging applications, prospects, and research value. Furthermore, it has a good adsorption effect on low-concentration ammonia nitrogen under laboratory simulation conditions and can therefore be applied in the future to decrease eutrophication in farmland water.

**Author Contributions:** Conceptualization, H.L. and Y.Z.; methodology, H.L., B.L. and X.T.; software, B.Y. and M.S.; validation, X.T. and B.L.; formal analysis, X.T. and Y.Z.; investigation, H.L., Z.L., M.S. and B.Y.; resources, Y.Z.; data curation, Z.L. and X.T.; writing—original draft preparation, Y.Z. and H.L.; writing—review and editing, X.T.; visualization, B.Y. and H.L.; supervision, X.T.; project administration, Y.Z.; funding acquisition, Y.Z. All authors have read and agreed to the published version of the manuscript.

**Funding:** This work was supported by Fundamental Research Funds for the Central Universities (451180304165), Environmental Protection Research Project of Ecology and Environment Department of Jilin Province (No. 2019-12), and Science and Technology Innovation Project (QDKY202001) of the 7th Institute of Geology & Mineral Exploration of Shandong Province.

**Institutional Review Board Statement:** Not applicable.

**Informed Consent Statement:** Not applicable.

**Data Availability Statement:** Data are contained within the article.

**Conflicts of Interest:** The authors declare no conflict of interest.

## References

- Ren, Z.; Jia, B.; Zhang, G.; Fu, X.; Wang, Z.; Wang, P.; Lv, L. Study on adsorption of ammonia nitrogen by iron-loaded activated carbon from low temperature wastewater. *Chemosphere* **2021**, *262*, 127895. [[CrossRef](#)] [[PubMed](#)]
- Ozturk, E.; Bal, N. Evaluation of ammonia-nitrogen removal efficiency from aqueous solutions by ultrasonic irradiation in short sonication periods. *Ultrason. Sonochem.* **2015**, *26*, 422–427. [[CrossRef](#)] [[PubMed](#)]
- Sotoft, L.F.; Pryds, M.B.; Nielsen, A.K.; Norddahl, B. Process Simulation of Ammonia Recovery from Biogas Digestate by Air Stripping with Reduced Chemical Consumption. *Comput. Aided Chem. Eng.* **2015**, *37*, 2465–2470.
- Zhu, G.-B.; Peng, Y.-Z.; Wu, S.-Y.; Wang, S.-Y.; Xu, S.-W. Simultaneous nitrification and denitrification in step feeding biological nitrogen removal process. *J. Environ. Sci.* **2007**, *19*, 1043–1048. [[CrossRef](#)]
- Huang, H.; Liu, J.; Ding, L. Recovery of phosphate and ammonia nitrogen from the anaerobic digestion supernatant of activated sludge by chemical precipitation. *J. Clean. Prod.* **2015**, *102*, 437–446. [[CrossRef](#)]
- Xiang, S.; Liu, Y.; Zhang, G.; Ruan, R.; Wang, Y.; Wu, X.; Zheng, H.; Zhang, Q.; Cao, L. New progress of ammonia recovery during ammonia nitrogen removal from various wastewaters. *World J. Microbiol. Biotechnol.* **2020**, *36*, 144. [[CrossRef](#)]
- Adam, M.R.; Othman, M.H.D.; Abu Samah, R.; Puteh, M.H.; Ismail, A.F.; Mustafa, A.; Rahman, M.A.; Jaafar, J. Current trends and future prospects of ammonia removal in wastewater: A comprehensive review on adsorptive membrane development. *Sep. Purif. Technol.* **2019**, *213*, 114–132. [[CrossRef](#)]
- Meng, X.; Khoso, S.A.; Jiang, F.; Zhang, Y.; Yue, T.; Gao, J.; Lin, S.; Liu, R.; Gao, Z.; Chen, P.; et al. Removal of chemical oxygen demand and ammonia nitrogen from lead smelting wastewater with high salts content using electrochemical oxidation combined with coagulation–flocculation treatment. *Sep. Purif. Technol.* **2020**, *235*, 116233. [[CrossRef](#)]
- Jorgensen, T.C.; Weatherley, L.R. Ammonia removal from wastewater by ion exchange in the presence of organic contaminants. *Water Res.* **2003**, *37*, 1723–1728. [[CrossRef](#)]
- Huang, X.; Zhao, H.; Zhang, G.; Li, J.; Yang, Y.; Ji, P. Potential of removing Cd(II) and Pb(II) from contaminated water using a newly modified fly ash. *Chemosphere* **2020**, *242*, 125148. [[CrossRef](#)]
- Sprynskyy, M.; Lebedynets, M.; Terzyk, A.P.; Kowalczyk, P.; Namiesnik, J.; Buszewski, B. Ammonium sorption from aqueous solutions by the natural zeolite Transcarpathian clinoptilolite studied under dynamic conditions. *J. Colloid Interface Sci.* **2005**, *284*, 408–415. [[CrossRef](#)]
- Huang, H.; Yang, L.; Xue, Q.; Liu, J.; Hou, L.; Ding, L. Removal of ammonium from swine wastewater by zeolite combined with chlorination for regeneration. *J. Environ. Manag.* **2015**, *160*, 333–341. [[CrossRef](#)]
- Hong, M.; Yu, L.; Wang, Y.; Zhang, J.; Chen, Z.; Dong, L.; Zan, Q.; Li, R. Heavy metal adsorption with zeolites: The role of hierarchical pore architecture. *Chem. Eng. J.* **2019**, *359*, 363–372. [[CrossRef](#)]
- Chen, X.J.; Guo, Y.X.; Cheng, F.Q.; Song, H.P.; Zheng, N.; Wang, X.M. Application of Modified Coal Fly Ash as an Absorbent for Ammonia-Nitrogen Wastewater Treatment. *Adv. Mater. Res.* **2012**, *518–523*, 2380–2384. [[CrossRef](#)]
- Mostafa Hosseini Asl, S.; Ghadi, A.; Sharifzadeh Baei, M.; Javadian, H.; Maghsudi, M.; Kazemian, H. Porous catalysts fabricated from coal fly ash as cost-effective alternatives for industrial applications: A review. *Fuel* **2018**, *217*, 320–342. [[CrossRef](#)]
- Dubey, S.; Sujaritanonta, L.; Sharma, Y.C. Application of fly ash for adsorptive removal of malachite green from aqueous solutions. *Desalin. Water Treat.* **2013**, *53*, 91–98. [[CrossRef](#)]
- He, K.; Chen, Y.; Tang, Z.; Hu, Y. Removal of heavy metal ions from aqueous solution by zeolite synthesized from fly ash. *Environ. Sci. Pollut. Res. Int.* **2016**, *23*, 2778–2788. [[CrossRef](#)]
- Gao, M.; Ma, Q.; Lin, Q.; Chang, J.; Bao, W.; Ma, H. Combined modification of fly ash with Ca(OH)<sub>2</sub>/Na<sub>2</sub>FeO<sub>4</sub> and its adsorption of Methyl orange. *Appl. Surf. Sci.* **2015**, *359*, 323–330. [[CrossRef](#)]
- Musyoka, N.M.; Petrik, L.; Hums, E. Synthesis of Zeolite A, X and P from a South African Coal Fly Ash. *Adv. Mater. Res.* **2012**, *512–515*, 1757–1762. [[CrossRef](#)]
- Penghamkeerati, P.; Satapanajaru, T.; Chularuengoaksorn, P. Chemical modification of coal fly ash for the removal of phosphate from aqueous solution. *Fuel* **2008**, *87*, 2469–2476. [[CrossRef](#)]
- Zhou, L.; Chen, Y.-L.; Zhang, X.-H.; Tian, F.-M.; Zu, Z.-N. Zeolites developed from mixed alkali modified coal fly ash for adsorption of volatile organic compounds. *Mater. Lett.* **2014**, *119*, 140–142. [[CrossRef](#)]
- Luo, Z.W.; Chen, Z.; Liu, S.H. A Study on Adsorption Ammonia Nitrogen of Diatomite Modified by Microwave. *Adv. Mater. Res.* **2012**, *602–604*, 1211–1214. [[CrossRef](#)]
- Wang, W.P.; Wang, W.; Zhou, Y.Q. Adsorption Characteristics of Natural Zeolite on Ammonia Nitrogen. *Adv. Mater. Res.* **2012**, *599*, 501–504. [[CrossRef](#)]
- Grismer, M.E.; Collison, R.S. The Zeolite-Anammox Treatment Process for Nitrogen Removal from Wastewater—A Review. *Water* **2017**, *9*, 901. [[CrossRef](#)]
- Chen, Y.; Wang, N.; An, S.; Cai, C.; Peng, J.; Xie, M.; Peng, J.; Song, X. Synthesis of novel hierarchical porous zeolitization ceramics from industrial waste as efficient adsorbent for separation of ammonia nitrogen. *Sep. Purif. Technol.* **2022**, *297*, 121418. [[CrossRef](#)]
- Zhang, L.; Wang, J.; Qiao, H.; Liu, F.; Fu, Z. Synthesis of manganese oxides for adsorptive removal of ammonia nitrogen from aqueous solutions. *J. Clean. Prod.* **2020**, *272*, 123055. [[CrossRef](#)]
- Yuan, J.; Zhu, Y.; Wang, J.; Liu, Z.; Wu, J.; Zhang, T.; Li, P.; Qiu, F. The application of the modified durian biomass fiber as adsorbent for effective removal of ammonia nitrogen. *J. Iran. Chem. Soc.* **2022**, *19*, 435–445. [[CrossRef](#)]

28. Chen, X.; Song, H.; Guo, Y.; Wang, L.; Cheng, F. Converting waste coal fly ash into effective adsorbent for the removal of ammonia nitrogen in water. *J. Mater. Sci.* **2018**, *53*, 12731–12740. [[CrossRef](#)]
29. Cheng, H.; Zhu, Q.; Xing, Z. Adsorption of ammonia nitrogen in low temperature domestic wastewater by modification bentonite. *J. Clean. Prod.* **2019**, *233*, 720–730. [[CrossRef](#)]
30. Wang, L.; Huang, X.; Zhang, J.; Wu, F.; Liu, F.; Zhao, H.; Hu, X.; Zhao, X.; Li, J.; Ju, X.; et al. Stabilization of lead in waste water and farmland soil using modified coal fly ash. *J. Clean. Prod.* **2021**, *314*, 127957. [[CrossRef](#)]
31. Nguyen, T.C.; Tran, T.D.M.; Dao, V.B.; Vu, Q.-T.; Nguyen, T.D.; Thai, H. Using Modified Fly Ash for Removal of Heavy Metal Ions from Aqueous Solution. *J. Chem.* **2020**, *2020*, 8428473. [[CrossRef](#)]
32. Zhao, X.; Zhao, H.; Huang, X.; Wang, L.; Liu, F.; Hu, X.; Li, J.; Zhang, G.; Ji, P. Effect and mechanisms of synthesis conditions on the cadmium adsorption capacity of modified fly ash. *Ecotoxicol. Environ. Saf.* **2021**, *223*, 112550. [[CrossRef](#)]
33. Guo, R.; Yao, W.; Ma, H.; Yuan, J. Two-step hydrothermal synthesis of nano-kaolinite from fly ash: Thermodynamics and mechanism. *J. Clean. Prod.* **2020**, *271*, 122567. [[CrossRef](#)]
34. Eteba, A.; Bassyouni, M.; Saleh, M. Utilization of chemically modified coal fly ash as cost-effective adsorbent for removal of hazardous organic wastes. *Int. J. Environ. Sci. Technol.* **2022**. [[CrossRef](#)]
35. Gao, C.; Yu, R.; Huang, J. Organic–inorganic hybridized zeolite by polycardanol for ammonia-nitrogen adsorption. *J. Disper. Sci. Technol.* **2019**, *42*, 319–327. [[CrossRef](#)]
36. Quezada, G.R.; Rozas, R.E.; Toledo, P.G. Ab Initio Calculations of Partial Charges at Kaolinite Edge Sites and Molecular Dynamics Simulations of Cation Adsorption in Saline Solutions at and above the pH of Zero Charge. *J. Phys. Chem. C* **2019**, *123*, 22971–22980. [[CrossRef](#)]
37. Jiang, X.; Fan, W.; Li, C.; Wang, Y.; Bai, J.; Yang, H.; Liu, X. Removal of Cr(vi) from wastewater by a two-step method of oxalic acid reduction-modified fly ash adsorption. *RSC Adv.* **2019**, *9*, 33949–33956. [[CrossRef](#)]
38. Sellaoui, L.; Gómez-Avilés, A.; Dhaouadi, F.; Bedia, J.; Bonilla-Petriciolet, A.; Rtimi, S.; Belver, C. Adsorption of emerging pollutants on lignin-based activated carbon: Analysis of adsorption mechanism via characterization, kinetics and equilibrium studies. *Chem. Eng. J.* **2023**, *452*, 139399. [[CrossRef](#)]
39. Ayawei, N.; Ebelegi, A.N.; Wankasi, D. Modelling and Interpretation of Adsorption Isotherms. *J. Chem.* **2017**, *2017*, 3039817. [[CrossRef](#)]

**Disclaimer/Publisher’s Note:** The statements, opinions and data contained in all publications are solely those of the individual author(s) and contributor(s) and not of MDPI and/or the editor(s). MDPI and/or the editor(s) disclaim responsibility for any injury to people or property resulting from any ideas, methods, instructions or products referred to in the content.